Indian Journal of Engineering & Materials Sciences
Vol. 23, October 2016, pp. 341-348

Numerical study of TTP curves upon welding of 6063-T5 aluminium alloy and optimization of welding process parameters by Taguchi´s method

José L Meseguer-Valdenebro*, Antonio Portoles & J Oñoro

Department of Applied Physics and Materials Engineering, School of Mechanical Engineering, Technical University of Madrid, C/ José Gutiérrez Abascal st, 2, 28006 Madrid, Spain

Received 7 May 2015; accepted 9 August 2016

This paper presents a numerical study to determine the cooling curves of 6063-T5 aluminium alloy plane plates using the MIG welding technique. The aluminium alloys show characteristic curves, known as time-temperature-property (TTP) curves, representing time-temperature-properties that indicate the mechanical properties obtained by the cooling process, and therefore the area of intersection between the cooling curve and the TTP curve quantitatively approximates the mechanical properties obtained in the welding joint. In addition, the mechanical properties in a welded aluminium alloy also depend on the time taken to cool the welding joint from 410°C to 300°C. The electrical parameters are the source power and welding speed, which are selected from the European welding standard to ensure adequate reproduction of results. In this work, the area of intersection between the cooling curve and $t_{4/3}$ is optimized by Taguchi's method, where the signal-to-noise ratio and analysis of variance are utilized to obtain the influence of the parameters on the area of intersection and $t_{4/3}$. This numerical study can also be applied to the GTAW welding technique.

Keywords: Aluminium alloy 6063-T5, Welding, Cooling time, Taguchi, Finite element method, Experimental design, TTP curve

Early last century, aluminium alloys were introduced when a mixture of aluminium with others elements was obtained in order to increase the mechanical properties of the aluminium. Further development of aluminium alloys was provided by duralumin, the generic name given to age-hard enable aluminium. The main alloying elements of aluminium alloys are copper, manganese, magnesium, and silicon[1].

The first age-hardened alloy was developed by Guinier-Preston[2] and consisted of an alloy of aluminium and copper named hard aluminium. This alloy ages at temperatures below room temperature due to the excess copper in its interior in the form of $CuAl_2$. There are two types of ageing processes: (i) natural ageing, where precipitates appear spontaneously on the surface of an alloy, and (ii) artificial ageing, which occurs due to an induced heat treatment at temperatures lower than the transformation temperature. Through both natural ageing and artificial ageing, a microstructure consisting of grains of phase α is obtained with a fine dispersion of results which are not visible with a light microscope[3].

*Corresponding author (E-mail: jlmeseguer507@gmail.com)

Therefore, alloys can be classified by the method used to increase their mechanical strength, making a distinction between non-heat-treatable[4,5] and heat-treatable alloys[6,7]. The first type is associated with alloys that have a second phase dispersion of elements in solid solution and that have been cold worked, whereas the second type is obtained by dissolving the alloying elements in a solid solution and subsequent precipitation of these small precipitates.

This manuscript aims to characterize the aluminium alloy 6063-T5, which belongs to the six thousand (6XXX) series and therefore contains magnesium and silicon, and therefore it is an alloy containing magnesium and silicon. Magnesium accelerates the precipitation reactions in the alloy by increasing the strength and hardness of the alloy[8].

The quality of the welding bead in aluminium welding is determined though its chemical composition and the solidification rate of the weld. A greater solidification speed occurs in very thick plates, so that as the plate thickness is reduced, the cooling rate becomes slower. The solidification rate in the joint characterizes the welding thermal cycle of the joint and therefore determines its mechanical quality[9]. There are two critical factors that determine

the quality of aluminium alloys: (i) the cooling time, also known as $t_{4/3}$, which is the time from 410°C to 300°C ($t_{4/3}$), which allow determining the ratio of β precipitates, which are not beneficial for the bead properties[10,11]; and (ii) the critical area, which is the area of intersection between the cooling curve and the time-temperature-property (TTP) curve, which determines the amount and kind of precipitates that appear in the welding joint[10]. As the area of intersection and $t_{4/3}$ increase, the precipitates obtained become bigger and therefore the mechanical properties will be worse and vice versa.

Several studies performed to determine $t_{4/3}$ and the critical area of aluminium alloy welding joints can be found in the scientific literature[12-14]. The critical area and $t_{4/3}$ may change according to the welding processes used, so each process has its own characteristics and therefore a different energy rate. The critical area and $t_{4/3}$ may change according to the welding processes used because each process has its own characteristics and therefore a different energy rate. The electric arc welding processes most commonly used to weld aluminium alloys are GTAW[15] and MIG[16]. The GTAW welding process can control the source energy at minimum values near the micro-arc, and is also known as micro-TIG[17].

The current work carries out a numerical study using the finite element method for the MIG welding process using 6063-T5 aluminium alloy in order to determine $t_{4/3}$ and the critical area. The influence of welding parameters is also studied through Taguchi's method[18]. Taguchi's method has been widely used by several authors, such as Kumal *et al.*[19], who studied the influence of welding parameters on the mechanical properties of AA5456 aluminium alloy using the TIG process, and Haragopal *et al.*[20], who studied the influence of welding parameters on the mechanical properties of Al-65032 aluminium alloy using the MIG process.

Experimental Design by Taguchi´s Method

Taguchi design, also known as orthogonal arrays, is a method used to design experiments that usually require only a fraction of the complete factorial combinations. An orthogonal array means that the design is balanced so that the factor levels are weighted equally, and thus each factor can be evaluated regardless of all other factors, so the effect of a factor does not influence the estimation of the other factors[18].

The experiments are conducted in accordance with the principles of Taguchi´s experimental method in order to determine the effects of the main parameters of the welding process. The parameters of the process that remain constant in each experiment are the protective gas flow (12 L/min), wire stick-out length (1 mm), the wire diameter (1 mm), and the bevel separation (1 mm). The process parameters are the welding speed and source power and are varied in each experiment. Table 1 shows the levels of the experimental design.

Through an orthogonal matrix, L4, Taguchi's method determines the number of experiments required for two variables[18], namely the power and welding speed. The computational study is developed for 6063-T5 aluminium alloy plates with dimensions of 50×150×2 mm^3. The process output variables are the cooling time $t_{4/3}$ and the critical area between the TTP curve and cooling time. The matrix of experiments is given in Table 2.

Thermal Analysis of Welded Joints

The thermal analysis by means of a finite elements model of the welding joint is based on the equation of transference of heat[21]:

$$\rho(T)\cdot c_p(T)\cdot\frac{\partial T}{\partial t}=q+\frac{\partial}{\partial x}\left[K_x(T)\cdot\frac{\partial T}{\partial x}\right]+\frac{\partial}{\partial y}\left[K_y(T)\cdot\frac{\partial T}{\partial y}\right]+\frac{\partial}{\partial z}\left[K_z(T)\cdot\frac{\partial T}{\partial z}\right] \quad \text{... (1)}$$

where $\rho(T)$ is the density of material, $c_p(T)$ is the specific heat, $q(T)$ is the heat generated per unit of volume, $K_x(T)$, $K_y(T)$, and $K_z(T)$ are thermal conductivity coefficients for three space directions, T is the temperature, and t is the time elapsed. The thermal behaviour is governed by a nonlinear differential equation because of the material's

Table 1 — Levels of welding process MIG

	Welding parameters	Units	Level 1	Level 2
P	Power	W	1557	1673
V_s	Welding speed	mm/s	11.5	12.25

Table 2 — Matrix of experiments

Experiment Nº	Welding parameters				
	Intensity (A)	Voltage (V)	P (W)	V_s[mm/s]	Thermal input(J/mm)
1	120	12.9	1557	11.5	135.39
2	120	12.9	1557	12.25	127.10
3	150	11.15	1673	11.5	145.47
4	150	11.15	1673	12.25	136.57

physical properties depend on temperature[15,16]. The representations of specific heat in Fig. 1 shows the change of phase from solid to fluid when the heat source melts the metal.

Modelling of thermalcycle

The geometry studied in this paper is composed of two plates (Fig. 2), without bevels and 1 mm thickness.

Plate mesh

The finite element software used in this paper is ANSYS R14.5. The thermal element used to mesh it is 'SOLID 70', which is composed of eight nodes[18,19]. Figure 3 shows the meshed plate. The mesh is structured so that its size changes from coarse mesh of 5 mm (at the ends of the plates) to fine mesh of 2 mm (in the centre of the plate). A mesh sensitivity analysis was carried out and the numbers of nodes and elements are 23020 and 3136, respectively.

Applied loads, contour conditions, and initial conditions

The generated heat loads (W/m^3) are applied on each of the sections that form the weld bead. The length of each section is proportional to the welding speed for 1 s. The value of the load in each section is equal to the quotient of the power of the source divided by the thermal efficiency and the volume of each of the sections that form the fillet weld. The thermal efficiency of the source is 75% according to Dupont *et al.*[28]. Figure 4 represents each of the sections that comprise the weld depending on the welding speed. The specific power for the four experiments is given in Table 3.

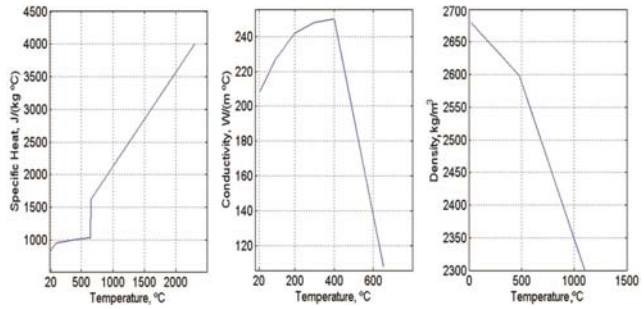

Fig. 1 — Properties of 6063-T5 aluminum alloy[24,25]

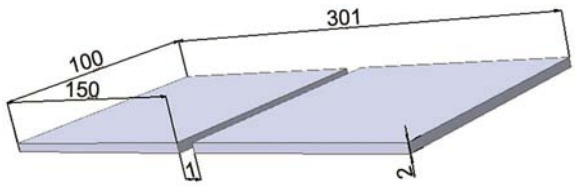

Fig. 2 — Sketch of plates and separation of bevels

The heat losses through radiation and convection are applied on the surfaces of the plates and are taken into account through the following relationship[21]:

$$q_c = h \cdot \left(T - T_\infty\right) \quad ...(2)$$

$$q_r = \varepsilon \cdot s \cdot \left(T^4 - T_\infty^4\right) \quad ...(3)$$

h (W/m^2 · ºC) is the convection coefficient, T_∞ (ºC) is the environmental temperature, ε is the body surface emissivity, and *s*is Stefan-Boltzmann's constant. Figure 5 shows the coefficients of convection and emissivity. The initial conditions are 25 ºC in all models.

TTP Curves

TTP curves are expressed analytically by Eq. (4) and determine the properties of the alloy based on the temperature and time. The kinetic coefficients of the TTP curves of the 6063-T5 alloy[29] are listed in Table 4.

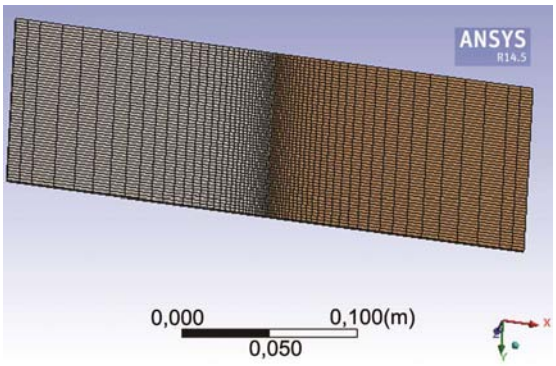

Fig. 3 — Meshed zones of plate and bead

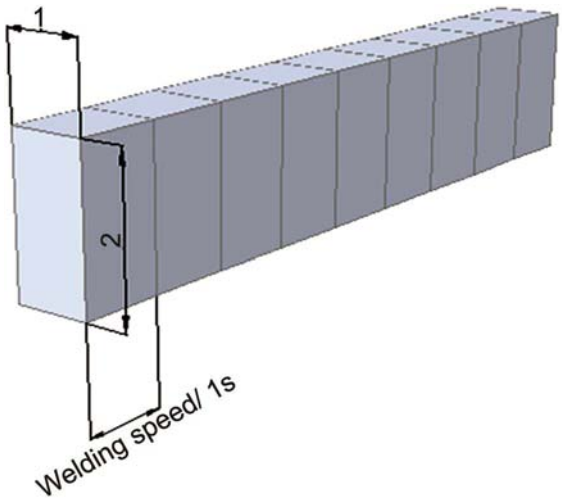

Fig. 4 — Sections size of the weld bead measured in mm

$$C_t = -k_1 \cdot k_2 \cdot \exp\left[\frac{k_3 \cdot k_4^2}{R \cdot T \cdot (k_4 - T)^2}\right] \cdot \exp\left(\frac{k_5}{R \cdot T}\right) \quad \ldots (4)$$

Where K_1 is the natural logarithm of the fraction that is not transformed during cooling, K_2 is the proportional constant to the nucleation (s^{-1}), K_3 is the energy necessary for the nucleation ($1/(J \cdot mol^{-1})$), K_4 is the constant of the solvus temperature (K^{-1}), K_5 is the constant of the activation energy by diffusion ($1/(J \cdot mol^{-1})$), R is the constant of gases ($J \cdot mol^{-1} \cdot K^{-1}$), and T is thetemperature (K).

The area of intersection between the cooling curve and the TTP curve represents the critical area. The size of the critical area obtained qualitatively determines the properties of the welded joint. If the area of intersection increases, the properties of the joint worsen, and if the area of the joint decreases, its properties improve.

Results and Discussion

Once the loads from Table 3 and the contour conditions from Fig. 5 have been applied, the results of the four experiments are obtained.

Table 3 — Specific power for the four experiments.

Experiment Nº	Power (W)	Welding speed $\cdot 10^{-3}$ (m/s)	Bead volume $\cdot 10^{-8}$ (m^3)	Specific power (W/m^3) 10^{10}
1	1557	11.5	2.3	5.08
2	1557	12.25	2.45	4.77
3	1673	11.5	2.3	5.46
4	1673	12.25	2.45	5.12

Table 4 — Coefficients of curve TTP for the alloy 6063-T5[29]

k_1	k_2 (s)	k_3 ($J \cdot mol^{-1}$)	k_4 (K)	k_5 ($J \cdot mol^{-1}$)
Ln(0.99)	$4.8 \cdot 10^{-10}$	4146	946	111627

Results of the modelling

Figure 6 presents the results of the modelling for the instant t = 8 s, where a maximum temperature equal to 1634ºC is reached. In other investigations, similar temperatures were obtained by means of electrical arc welding of the aluminium alloy 6063-T5[30].

Cooling curves and $t_{4/3}$

Figure 7 shows the four cooling curves of the weld bead measured 70 mm from the end of the plate. The cooling time is shown on the abscissa axis and the temperature is shown on the ordinate axis.

Table 5 gives the largest value of $t_{4/3}$, followed by experiments 1 and 4, which give intermediate values of $t_{4/3}$, while experiment 2 presents the shortest cooling time.

Table 5 verifies that the energy of the source increases $t_{4/3}$, and therefore there is a loss of mechanical properties in the welding joint due to the high energy source values. The energy of the source is calculated by means of Eq. (5).

$$E = \frac{Power}{velocity} \quad \ldots (5)$$

Critical area

The critical area of intersection is determined by means of the intersection between the cooling curve and the TTP curve. The size of the critical area of intersection is calculated by means of the trapeze rule[31]. Figure 8 shows the intersection between the cooling curve and the TTP curve for experiment 1. The points of intersection of the cooling curve and the TTP curve with respect to the ordinate axis are

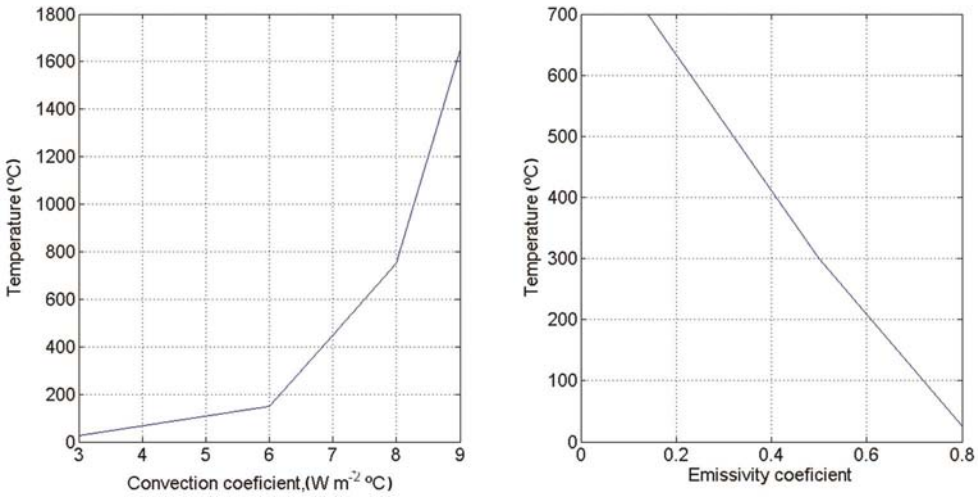

Fig. 5 — Coefficients of convection and emissivity applied[24,25]

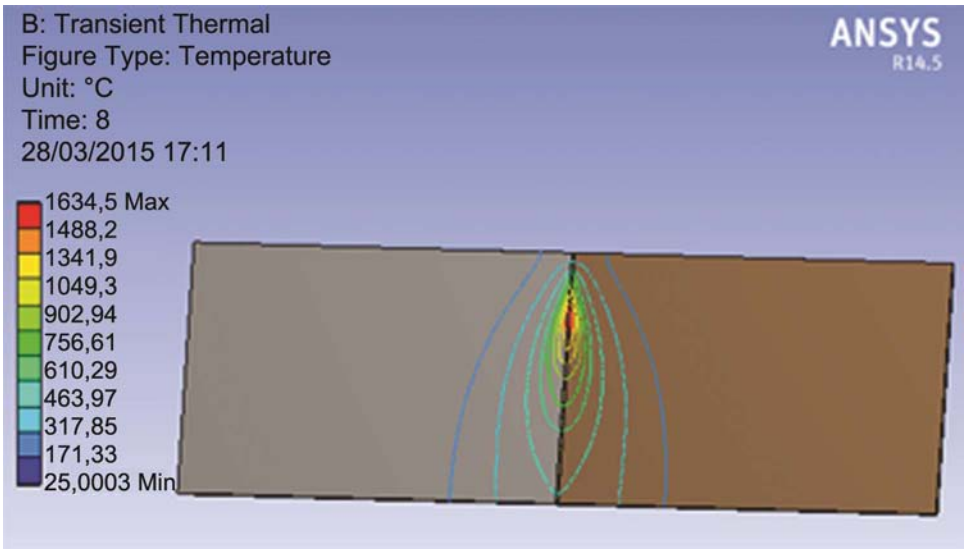

Fig. 6 — Modeling by ANSYS of the experiment 1 welding joint

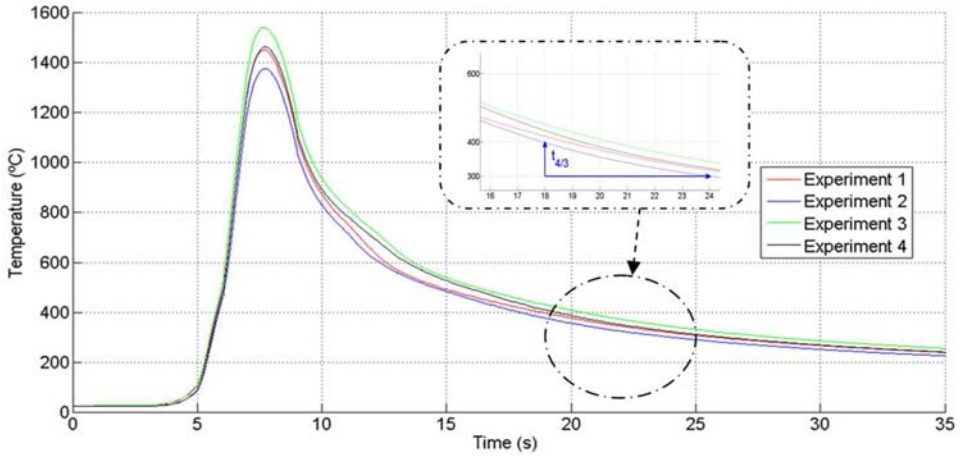

Fig. 7 — Cooling curves of the four experiments of alloy 6063-T5

Table 5 — Cooling time $t_{4/3}$ versus Energy

Experiment Nº	Power (W)	Welding speed · 10^{-3} (m/s)	Energy · 10^5 (J/s)	$t_{4/3}$ (s)
1	1557	11.5	1.02	6.87
2	1557	12.25	0.95	6.01
3	1673	11.5	1.09	7.67
4	1673	12.25	1.02	6.63

between approximately 400°C and 300ºC, and the area between the TTP curve and the cooling curve shows qualitatively the amount of precipitates at the point measured according to the cooling time $t_{4/3}$.

Figure 9 shows the intersection between the cooling curve and the TTP curve for the four proposed experiments. Table 6 gives the areas of intersection for the four experiments. From Table 6, it can be seen that the maximum size of the area of intersection is obtained in experiment 2 and the minimum size is obtained in experiment 4. Therefore, the optimum area is that obtained in experiment 2, which gives the minimum area.

Figure 10 illustrates the linear relationship between $t_{4/3}$ and the critical area. The relationship between the results is similar in each experiment; that is, if $t_{4/3}$ increases, the critical area increases, and vice-versa, and therefore there is a relationship between the critical area and $t_{4/3}$.

Taguchi Optimization

Taguchi optimization determines the influence of each of the variables on $t_{4/3}$ and the critical area using the criterion "the smaller the better". Equation (6) is the equation used to calculate the signal-to-noise ratio (S/N) [32].

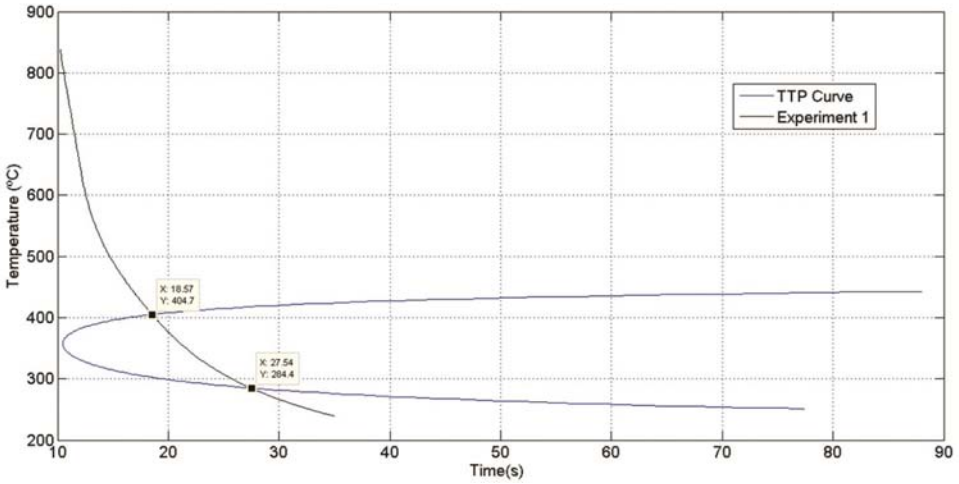

Fig. 8 — Area intersected for experiment 1

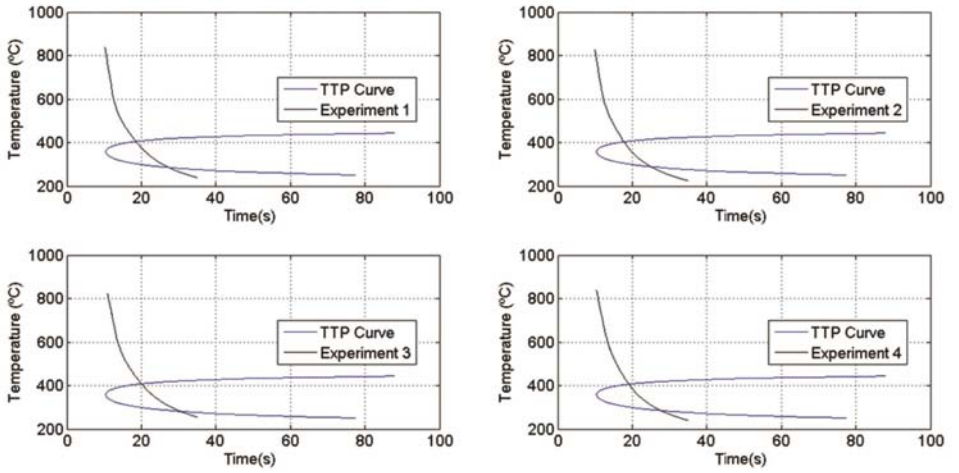

Fig. 9 — Representing intersecting areas for each of the experiments

Table 6 — Intersected areas for each experiment

Experiment Nº	Power (W)	Welding speed · 10^{-3} (m/s)	Energy · 10^5 (J/s)	Area (ºC · s)
1	1557	11.5	1.02	348.06
2	1557	12.25	0.95	287.41
3	1673	11.5	1.09	418.48
4	1673	12.25	1.02	356.75

$$\frac{S}{N} = -10 \cdot \log\left(\sum\left(Y^2\right)/n\right) \quad \ldots (6)$$

Y^2 are the sample values squared, and n is the sample size.

Table 7 gives the values of S/N for $t_{4/3}$ and the critical area. The minimum absolute value obtained is the optimal one. The optimal values of the power and welding speed with respect to $t_{4/3}$ and the critical area are given in Table 8. The optimal values correspond to the minimum power and the maximum welding speed required obtaining the minimum energy values, and both cases correspond to experiment number 2.

Analysis of variance

The relative effect of the welding parameters was studied by an analysis of variance (ANOVA)[33]. The objective of ANOVA is to quantify the importance of the welding parameters for the critical size area and $t_{4/3}$, that is, the relevance of the different welding parameters for the welding quality. Tables 9 and 10 show the ANOVA for the two cases.

The p-values in Table 9 are more significant than those in Table 10, because the former are smaller than the latter. Therefore, the results for the critical areas are more representative than the $t_{4/3}$ results. Figure 11 shows that both power and welding velocity have a similar influence on $t_{4/3}$ and the critical area; that is,

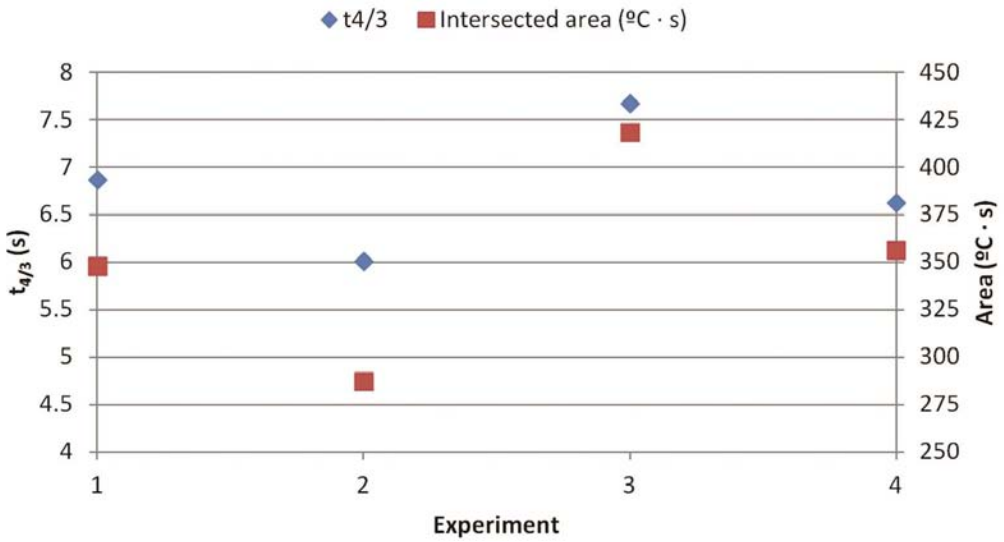

Fig. 10 — Representation of $t_{4/3}$ – Intersected area

Table 7 — Table of answers for S/N ratio

	$t_{4/3}$ (s)		Area (ºC · s)	
Level	P (W)	V_s (mm/s)	P (W)	V_s (mm/s)
1	-16.16	-17.22	-50.00	-51.63
2	-17.06	-16.00	-51.74	-50.11
Rank	2	1	1	2

Table 8 — Optimal values of power and welding speed to obtain the minimum $t_{4/3}$ and the minimum critical area

	Power (W)	Welding speed (mm/s)	Experiment Nº
Critical area (ºC · s)	1557	12.25	2
$t_{4/3}$ (s)	1557	12.25	2

Table 9 — Results of the ANOVA for the critical area

	Degrees of freedom	Sum of squares	Mean of squares	F	p-value
Power (W)	1	4883,21	4883,21	16746,30,0049194	
Velocity (mm/s)	1	3744,22	3744,22	12840,20,0056180	
Error	1	0,29	0,29		
Total	3	8627,72			

Table 10 — Results of the ANOVA for the $t_{4/3}$

	Degrees of freedom	Sum of squares	Mean of squares	F	p-value
Power (W)	1	0.5041	0.5041	62.235	0.0802
Velocity (mm/s)	1	0.9025	0.9025	111.420	0.0601
Error	1	0.0081	0.0081		
Total	3	1.4147			

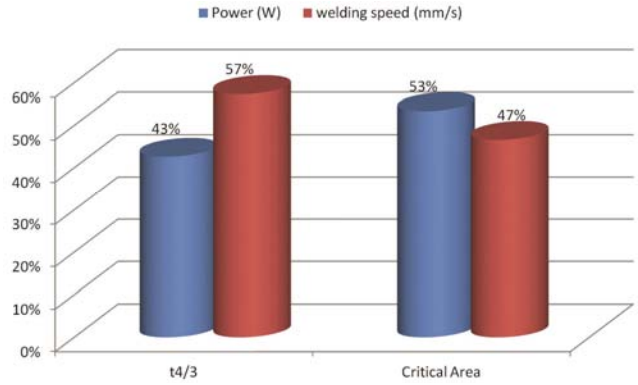

Fig. 11 — Influence of power and welding speed on critical area and $t_{4/3}$

the welding parameters of power and welding velocity affect both $t_{4/3}$ and the critical area in the same proportion around 50%.

Conclusions

The present work has studied the influence of the MIG welding parameters on $t_{4/3}$ and the critical area numerically. In order to use a criterion in the design of experiments (DOE), Taguchi's method has been used. The DOE has two parameters (power and welding speed) and two levels of each, and therefore an L4 array has been used. First, $t_{4/3}$ and the critical area are calculated. The value of $t_{4/3}$ and the critical area change with respect to the energy. If the value of energy is high, $t_{4/3}$ and the critical area decrease and if the value of energy is low, they increase. The critical area and $t_{4/3}$ change with respect to the energy. Secondly, the optimization of welding parameters

determined that the optimal experiment is the second one, which corresponds to a smaller value of energy. Finally, ANOVA was used to determine the significance of the studied welding parameters on $t_{4/3}$ and the critical area according to the *p*-value. The influence of power on $t_{4/3}$ and the critical area was 43% and 53%, respectively. From this, it is deduced that the influences of power and velocity are similar. However, the analysis realized by ANOVA determined that the influence on the critical area is more reliable than that on $t_{4/3}$.

Nomenclature

c_p	=	caloric capacity, [J kg^{-1} ºC]
$K_{x,y,z}$ *(T)*	=	Fourier conductivity of main directions , [W m^{-1} ºC^{-1}]
K_1	=	natural logarithm of the fraction non-transformed during the cooling
K_2	=	proportional constant to the nucleation, [s^{-1}]
K_3	=	necessary energy for the nucleation, [1/(J·mol^{-1})]
K_4	=	constant of the solvus temperature, [K^{-1}]
K_5		constant of the activation energy by diffusion, [1/(J·mol^{-1})]
N	=	sample size
P	=	power of the electric arc, [W]
p-value	=	probability of obtaining a test statistic result
q(T)	=	generated heat per unit of volume [J · m^{-3}]
q_c	=	convection heat [W·m^{-2}]
q_r	=	radiation heat [W·m^{-2}]
R	=	constant of gases, [J·mol^{-1}·K^{-1}]
s	=	Stefan-Boltzman's constant, [W · m^{-2} · ºC]
T	=	temperature, [K]
t	=	time [s]
$t_{4/3}$	=	cooling time between 400ºC and 300ºC
T_∞	=	environmental temperature, [ºC]
T_f	=	fusion temperature, [ºC]
v_s	=	welding speed, [m/s]
Y^2	=	sample values on squared
Greek letters		
ε	=	body surface emissivity
ρ	=	density, [kg m^{-3}]
Acronyms		
ANOVA	=	variance analysis
DOE	=	design of experiments
GMAW	=	gas metal arc welding
GTAW	=	gas tungsten arc welding
MIG	=	metal inert gas
S/N	=	signal to noise ratio
TIG	=	tungsten inert gas
TTP	=	time-temperature-properties

References

1 *ASM Handbook*, ASM International, USA, 2 (2002).
2 Singh C V& Warner D H, *Acta Mater*, 58 (17) (2010) 5797-5805.
3 Siddiqui R A, Abdullah H A & Al-Belushi K R, *J Mater Process Technol*, 102 (1-3) (2000) 234-240.
4 Furu T, Rsund R & Nes E, *Mater Sci Eng*, 214 (1-2) (1996) 122-132.
5 Jr R E S, Baumann S F & H C S, *Wrought Non–Heat-Treatable Aluminum Alloys*, in *Aluminum Alloys—Contemporary Research and Applications*, edited by Vasudevan A K & Doherty R D, vol 31 (Elsevier), 1989, 65-105.
6 Cavazos J L & Colás R, *Mater Charact*, 47 (3-4) (2001) 175-179.
7 JR E A S , *Heat-Treatable Aluminum Alloys*, in *Aluminum Alloys—Contemporary Research and Applications*, edited by Vasudevan A K & Doherty R D, vol 31 (Elsevier), 1989, 35-63.
8 Haupin W, in *Encyclopedia of Physical Science and Technology,* edited by Meyers R A, 3rd ed,(Academic Press, New York), 2003, 495-518.
9 Grong, *Metallurgical modelling of welding*, 2nd ed (The Institute of Materials, London), 1997.
10 Li H, Zeng C, Han M, Liu J & Lu X, *Trans Nonferrous Met Soc China*, 23 (1) (2013) 38-45.
11 Milkereit B, Wanderka N, Schick C & Kessler O, *Mater Sci Eng,* 550 (2012) 87-96.
12 Evancho J W & Willey L A, *Met Trans*, 5 (1974) 43-47.
13 Milkereit B, Giersberg L, Kessler O & Schick C, *Materials*, 7 (4) (2014) 2631-2649.
14 Shabestari S G, Malekan M, Gao M, Wang M, Wen L & Li G, *Can Met Q*, 1 (3-4) (2005-2012) 165-169.
15 Yarmuch M A R & Patchett B M, *Weld J*, 86 (7) (2007) 196S-200S.
16 Miguel V, Martinez-Conesa E J, Segura F, Manjabacas M C & Abellan E, *Rev Met*, 48 (5) (2012) 333-350.
17 Wang J, Kusumoto K & Nezu K, *Sci Technol Weld Join*, 9 (1) (2004) 90-94.
18 Roy R K, *Design of experiments using the Taguchi approach: 16 steps to product and process Improvement*, 1st ed. (Wiley Interscience, USA), 2001.
19 Kumar A & Sundarrajan S, *Optimization of pulsed TIG welding process parameters on mechanical properties of AA 5456 Aluminum alloy weldments*, (Apr. 2009) 1288–1297.
20 Haragopal G, Reddy P V R R, Reddy G C M & Subrahmanyam J V, *J Sci Ind Res*, 70 (10) (2011) 844-850.
21 Zhu X K & Chao Y J, *Comput Struc*, 80 (11) (2002) 967- 976.
22 Powell R W, Ho C Y & Liley P E, *Thermal conductivity of selected materials*, NSRDS, 1966.
23 CEN Technical Committee, *Eurocode 9: Design of aluminium structures. Part 1-1. General Rules*. BSI, 2000.
24 Francis J, *Welding simulations of aluminum alloy joints by finite element analysis*, Faculty of the Virginia Polytechnic Institute, Virginia, 2002.
25 Incropera F DeWitt D, Bergman T & Lavine A, *Fundamentals of Heat and Mass Transfer*, 6th ed (John Wiley & Sons, USA), 2007.
26 Moraitis G A& Labeas G N, *J Mater Process Technol*, 198 (1-3) (2008) 260-269.
27 Becerra A C, *Simulação Numérica da Soldagem com Aplicação à Caracterização do comportamento Dinâmico de Estruturas Soldada*s, Universidad Federal de Uberlândia, Brasil, 2006.
28 Dupont J & Marder A, *Weld J* , 74 (12) (1995) S406-S416.
29 Li H, Zeng C, Han M, Liu J & Lu X, *Trans Nonferrous Met Soc China*, 23 (1) (2014) 38-45.
30 Meseguer-Valdenebro J L, MartÃ-nez-Conesa E J, Serna-Serrano J & Portoles A, *Therm Sci*, 4 (2014) 106-116.
31 Eggert N & Lund J, *J Comput Appl Math*, 27 (3) (1989) 389-406.
32 *Minitab 16*. Minitab Inc, 2010.
33 Bozkurt Y, *Mater Des,* 35 (2012) 440-445.